This is the accepted manuscript made available via CHORUS. The article has been published as:

Insights into the laser-assisted photoelectric effect from solid-state surfaces

Lukas Wenthaus, Nikolay M. Kabachnik, Mario Borgwardt, Steffen Palutke, Dmytro Kutnyakhov, Federico Pressacco, Markus Scholz, Dmitrii Potorochin, Nils Wind, Stefan Düsterer, Günter Brenner, Oliver Gessner, Serguei Molodtsov, Wolfgang Eberhardt, and Friedrich Roth

Phys. Rev. B **110**, 235406 — Published 5 December 2024

DOI: 10.1103/PhysRevB.110.235406

New insights into the laser-assisted photoelectric effect from solid-state surfaces

Lukas Wenthaus,[1,*] Nikolay M. Kabachnik,[2,3] Mario Borgwardt,[4] Steffen Palutke,[1] Dmytro Kutnyakhov,[1] Federico Pressacco,[1] Markus Scholz,[1] Dmitrii Potorochin,[5,6] Nils Wind,[7] Stefan Düsterer,[1] Günter Brenner,[1] Oliver Gessner,[4] Serguei Molodtsov,[2,5,6] Wolfgang Eberhardt,[1] and Friedrich Roth[5,6,†]

[1] *Deutsches Elektronen-Synchrotron DESY, Notkestrasse 85, 22603 Hamburg, Germany*

[2] *European XFEL GmbH, Holzkoppel 4, 22869, Schenefeld, Germany*

[3] *Donostia International Physics Center(DIPC), E-20018 San Sebastian/Donostia, Spain*

[4] *Chemical Sciences Division, Lawrence Berkeley National Laboratory, Berkeley, California 94720, USA*

[5] *Institute of Experimental Physics, TU Bergakademie Freiberg, Leipziger Strasse 23, 09599 Freiberg, Germany*

[6] *Center for Efficient High Temperature Processes and Materials Conversion (ZeHS), TU Bergakademie Freiberg, Winklerstrasse 5, 09599, Freiberg, Germany*

[7] *Universität Hamburg, Luruper Chaussee 149, 22761, Hamburg, Germany*

(Dated: October 31, 2024)

Abstract

Photoemission from a solid surface provides a wealth of information about its electronic structure and dynamic evolution. Ultrafast pump-probe experiments offer real-time access to photon-surface interactions and the resulting electron dynamics. Here, we present a femtosecond time-resolved photoelectron spectroscopy study of laser-assisted photoemission (LAPE) from two different metal surfaces, tungsten and platinum. Utilizing synchronized IR laser and X-ray pulses, photoelectron sideband generation up to the sixth order is observed. A significant material-dependent variation of the LAPE response is not predicted by previous theoretical models. The observed phenomena are semi-quantitatively reproduced by considering distinct dynamic dielectric responses of the two materials. These findings provide a deeper understanding of the LAPE process and new insights into the dynamic interplay between optical laser fields and metal surfaces.

* lukas.wenthaus@desy.de

† friedrich.roth@physik.tu-freiberg.de

I. INTRODUCTION

Photoemission of electrons from atoms, molecules, and condensed matter provides the experimental basis of our understanding of electronic structure. Over the past fifty years, photoelectron spectroscopy (PES) has become one of the most widely used methods for materials characterization and investigation, and is now an essential analytical tool for probing the properties and working principles of materials and their functional interfaces. The technique combines high spectral resolution with the momentum selectivity and atomic-site specificity of valence- and core-electron emission. It can thus provide direct information on electronic band dispersions in energy-momentum space as well as on the local chemical and structural environment of atoms.

Over the past ~ 20 years, time-domain X-ray spectroscopy techniques have gained increasing attention in a variety of scientific communities due to their potential to reveal details of fast dynamic processes in matter that are not accessible in static X-ray experiments or by optical time domain probes. By using the pulsed time structure of X-ray light sources, pump-probe schemes have been introduced to probe local electronic structure changes.

Among the various available X-ray probe schemes, time-resolved photoelectron spectroscopy (tr-XPS) is particularly well suited to study ultrafast processes at surface and interfaces [1, 2]. In tr-XPS, a pump pulse typically excites a ground state configuration of the system under investigation, which is monitored by a time-delayed X-ray probe pulse, mapping the system's electronic dynamics onto an energy-resolving photoelectron detector.

When an electron is photo-emitted from an atom, molecule or solid in the presence of an intense optical laser field, an additional interaction can be observed. Whenever the X-ray pulse and the laser pulse coincide in time and space, the presence of the optical laser field modifies the photoelectron spectrum, leading to a redistribution of photoemission signal intensity and to the generation of multiple, equidistant peak structures termed sidebands (SBs). These replicas of the main photoemission peak are energetically separated from the main line by integer multiples of the laser photon energy. This two-color photoionization phenomenon is called the laser-assisted photoelectric effect (LAPE) and can be described as the simultaneous absorption or emission of one or more optical laser photons in the X-ray photoionization continuum.

Since its first experimental demonstration in noble gas atoms [3, 4], the X-ray LAPE pro-

cess has become a well-established technique to study ultrafast electronic processes in gas phase atoms and molecules and an essential tool for attosecond science [5, 6] or in the concept of Floquet engineering to coherently create new states of matter [7]. The transfer of the technique into the solid-state domain [8] introduced it as a standard method to determine the temporal overlap of X-ray and IR lasers in time-resolved photoemission experiments [1, 9] as well as a tool for pulse and data diagnostic [10–13]. Despite its widespread application, a comprehensive description and fundamental understanding of the intricate details of the LAPE processes is still missing. This is of crucial importance for many FEL-based experiments, since the appearance of sidebands is often part of the dynamic change in the recorded spectra that needs to be considered.

The redistribution of photoelectrons into sidebands can be seen as a spectral distortion overlapping with the actual physical effect of interest such as ultrafast photopeak shifts induced by charge transfer processes [2, 14–16]. The possibility of such phenomena occurring simultaneously requires special attention in detailed modeling of the underlying physical phenomena in order to separate the different contributions.

This is particularly important as emerging light source technologies provide more and more brilliant and shorter X-ray pulses that will, with the simultaneous improvement on the detector side, lead to considerably higher spectral and temporal resolution experiment. Furthermore, the need for correspondingly shorter optical laser pulses matching the X-ray pulse properties will increase peak intensities so that even at moderate photon fluences laser-induced shifts (e. g. AC Stark shifts) and pronounced LAPE effects become apparent.

Most reported LAPE measurements on solid and liquid systems were conducted using high-harmonic generation (HHG) light sources with comparatively low photon energies. These typically limit the spectral window to valence excitations that are often challenging to interpret due to their spectrally broad nature and complex structure [8, 17]. Combined with the relatively low kinetic energy of the photoelectrons, a precise modeling of the LAPE effect so far remained elusive.

This work presents the first systematic investigation of dynamic screening by time-resolved, laser-assisted XPS of shallow core levels of metallic solids, which is employed to monitor local electric fields at clean Pt (111) and W (110) single crystal surfaces. The experiment was conducted at the X-ray Free-Electron Laser FLASH in Hamburg [18] using a photon energy

of 514.5 eV. Comparison of the sideband formation in these two metals measured under identical experimental conditions reveals an unexpected dependence of the number of sidebands on the target material. The significantly different responses are attributed to electronic screening and the modification of the local electric fields at the clean Pt (111) and W (110) single crystal surfaces. The simple spectral shape and the high kinetic energy of core-level photoelectrons allow us to gain a deeper understanding and improve the modeling of the LAPE effect to derive a semi-quantitative explanation of the observed phenomenon. Moreover, the observed sensitivity of LAPE measurements to the dynamic dielectric response of the sample in the surface region paves the way to monitor electronic and/or lattice dynamics in this region using the extreme site-specificity provided by XPS.

II. EXPERIMENTAL

The tr-XPS experiment was carried out at the plane-grating monochromator beamline (PG2) at FLASH [19, 20], using the photoemission end-station WESPE (Wide-angle Electron SPEctrometer). A SPECS Themis 1000 time-of-flight analyzer equipped with a segmented, position-sensitive delay-line detector (DLD8080-4Q, Surface Concept) was used to record the photoelectron spectra. FLASH was operated at a fundamental wavelength of 7.5 nm with an effective repetition rate of 4 kHz (pulse trains of 400 pulses each with an intra-train repetition rate of 1 MHz and a train repetition rate of 10 Hz). The monochromator was operated with the 1200 lines/mm plane grating, a fix-focus constant (c_{ff}) of 2, and was tuned to the third harmonic of the FLASH fundamental in first diffraction order. A photon energy of 514.5 eV was used, with a bandwidth of 80 meV. The FEL pulse length on the sample was $\sim$140 fs (FWHM). This value includes the temporal broadening induced by the monochromator grating. The samples are exposed to $\sim$100 fs (FWHM) long IR laser pulses with a center wavelength of 1030 nm. They are generated in the PIGLET laser system [11] that is operated with the same pulse pattern as FLASH. The laser beam size was, under normal incidence, measured to be 220 μm x 270 μm with an X-ray beam size of about 70 μm x 70 μm, ensuring good spatial overlap and homogeneous laser intensities across the probed sample area. For the measurements the FEL and optical laser impinge colinear under an incidence angle of 55° with respect to the sample surface normal. The spectrometer is tilted by 55° in the horizontal direction with respect to the incoming beam and thereby detect electrons

emitted under normal emission within an acceptance cone of $\pm 7°$. Both, FEL and optical laser, provide p-polarization, which especially for the optical laser, provides a sample out-of-plane field component that is necessary for the sideband formation [17, 21]. To take care on static space charge effects [9], induced by the FEL, special care was taken to adjust the FEL intensity prior to the measurements. Optical induced dynamic space charge effects [22] are ruled out by careful adjustment of the optical laser fluence. To fulfill this requirement for both samples the value on target during the measurement was $\sim 1.2\,\mathrm{mJ/cm^2}$.

Two different sample materials, platinum (Pt) and tungsten (W), were selected to perform the LAPE experiments. Both 4f transition metals lend themselves to high-resolution sideband measurements - due to the small energy spread of the 4f-1 ionic. Both samples were cleaned by standard procedures: The Pt (111) crystal by repetitive cycles of Ar^+-sputtering and annealing, the W (110) crystal by annealing in an oxygen atmosphere and using high temperature flashes.

III. RESULTS AND DISCUSSION

We measured tr-XPS on W(110) and Pt(111) single crystal at the PG2 beamline at FLASH to investigate the material depended strength of the LAPE effect. Figure 1 (a) shows femtosecond time-resolved X-ray photoemission spectra of W 4f photolines as a function of time-delay (vertical) and binding energy (horizontal). The pump-probe delay range is $\pm\,0.5\,\mathrm{ps}$, whereby negative values are associated with the FEL pulse arriving before the optical laser pulse. The two main features at 31.6 eV ($4f_{7/2}$) and 33.8 eV ($4f_{5/2}$) correspond to the two spin-orbit components of the W 4f core-level. The unperturbed photoelectron spectrum is significantly modified under the presence of the IR laser field. This is depicted in Fig. 1 (c) by a lineout extracted from Fig. 1 (a) at a pump-probe delay of 0 ps. Distinct sidebands up to the sixth order appear on both sides of the central main peak, separated from it by integer mutiples of the IR photon energy (1.2 eV). For the W $4f_{7/2}$ line, the energy positions of the sidebands are indicated by boxes with different colors (cf. SB 1 - SB 6 in Fig. 1 (a) and (c)).

For comparison, Fig. 1 (b) and (d) show tr-XPS spectra for Pt (111) recorded under the same experimental conditions. As the measurement geometry, as well the FEL and optical wavelength was fixed, a major focus here was to maintain the laser fluence of $\sim 1.2\,\mathrm{mJ/cm^2}$

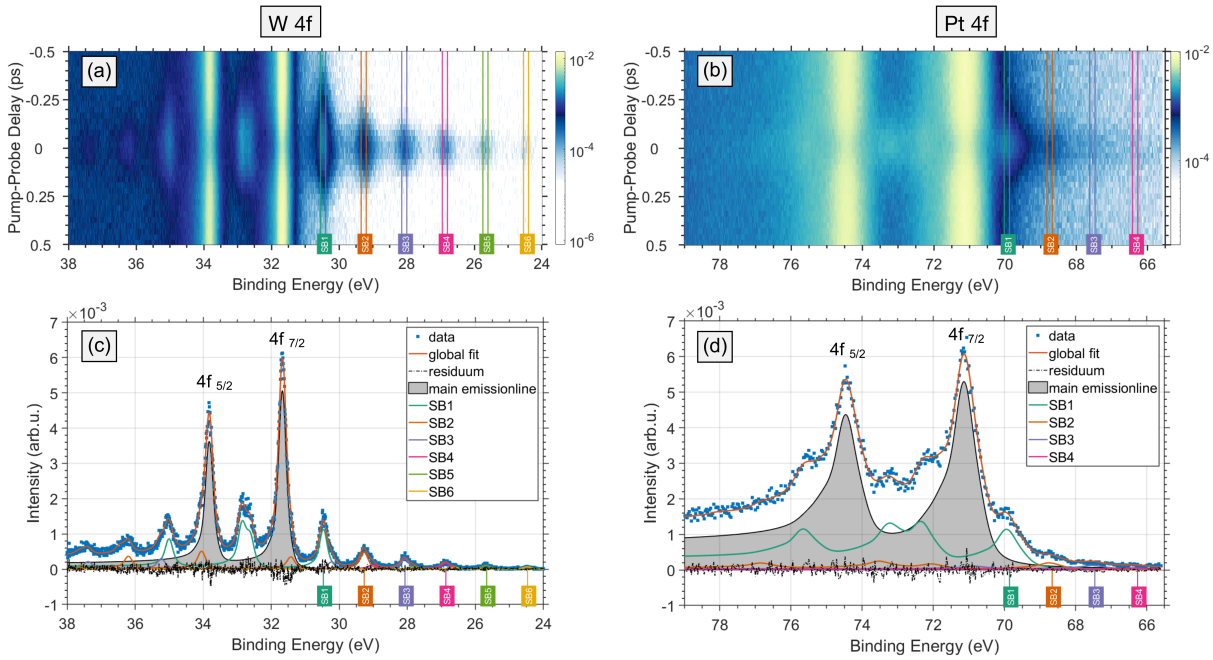

FIG. 1: Femtosecond time-resolved XPS spectra of the (a) W 4f and (b) Pt 4f photolines as a function of time-delay (vertical) and binding energy (horizontal). (c) and (d) Photoelectron spectra of the W 4f and Pt 4f core-level obtained at the temporal overlap at 0 ps (blue marker). The red line represents a convolution of the unperturbed photoelectron spectrum with the response function (RF). The black dashed line indicates the difference between the fit and the data.

to produce comparable data for both samples. Again, the full pump-probe dataset (see Fig. 1 (b)) is dominated by the two spin-orbit components of the 4f core-level located at 71.2 eV ($4f_{7/2}$) and 74.5 eV ($4f_{5/2}$). Similar to the tungsten measurement, sidebands are observed in the region of temporal overlap between the optical pump and the X-ray probe pulse (see Fig. 1 (d)). However, a closer inspection of the results for W (110) and Pt (111) reveals significant differences.

First, the main photolines and sidebands have different widths in the energy domain, whereby the W 4f lines are significantly narrower compared to the Pt 4f lines. This difference can be mainly explained by the different life-time widths of the 4f vacancies in W and Pt. Indeed, according to XPS measurements, the width of the $4f_{7/2}$ vacancy in Pt is about 5 times larger than in W (see, for example [23] and references therein). It is caused by strongly different probability of Coster-Kronig transitions in these two ions which determine

the width. We note that for both materials surface core-levels could not be distinguished because of the reduced surface sensitivity at the chosen excitation energy of 514.5 eV.

Second, the number of sidebands observed under identical experimental conditions differs significantly for the two materials. For tungsten, we observe sidebands up to the sixth order, whereby for platinum the maximum observe sideband order is four. This observation is surprising and has never been reported before. We note that the kinetic energy of the 4f photoelectrons in both cases is comparable (439 eV for Pt and 479 eV for W), and it is much larger than the energy of the IR photons. Below, we provide a semi-quantitative explanation of such a difference and show that the difference in the number of sidebands is related to the different optical properties of solid materials.

To quantify the observed LAPE effects, we use a phenomenological description similar to the one used in [8]. In a first step the unperturbed emission line was fitted. Here, a dataset well before the temporal overlap of optical and FEL pulses, between -0.9 ps and -0.7 ps delay, was selected to ensure the reference spectra are not impacted by the optical laser. The fit was done simultaneously for both spin-orbit components with a Doniach-Sunjic shape [24] representing the natural line-shape of the tungsten 4f core-levels. This line shape was convoluted with a Gaussian function to consider the energy broadening induced by the spectrometer and the X-ray photon energy spread after the monochromator.

Reminiscent of the approach in [8], we convoluted the unperturbed photoemission spectrum with a response function, which consists of a series of Gaussian shaped functions spaced by the laser photon energy $\hbar\omega_{IR}$. The response function reads:

$$RF(E) = \left(\frac{1 - \sum_{j=1,\pm}^{n} A_{j,\pm}}{\sqrt{2\pi\sigma^2}} \right) e^{-(E-E_0)^2/2\sigma^2} + \sum_{j=1,\pm}^{n} \frac{A_{j,\pm}}{\sqrt{2\pi\sigma^2}} e^{-(E-E_{0,SB}\pm j\hbar\omega_{IR})^2/2\sigma^2}. \quad (1)$$

Here, the first term replicates the unperturbed spectrum at energy E_0 with the intensity reduced by the fraction of electrons that populate the sidebands. The second term represents the sidebands, which are described by scaled copies of the central peak, shifted in energy by integer multiples of the IR photon energy. The Gaussian functions used to describe the sideband peaks are separated in energy by integer values of the optical photon energy and they are broadened with a width σ that reflects laser related specifics such as the spectral bandwidth and space charge effects. All scaling factors $A_{j,\pm}$ are determined with the overall photoemission intensity remaining constant. A fit with the above response function

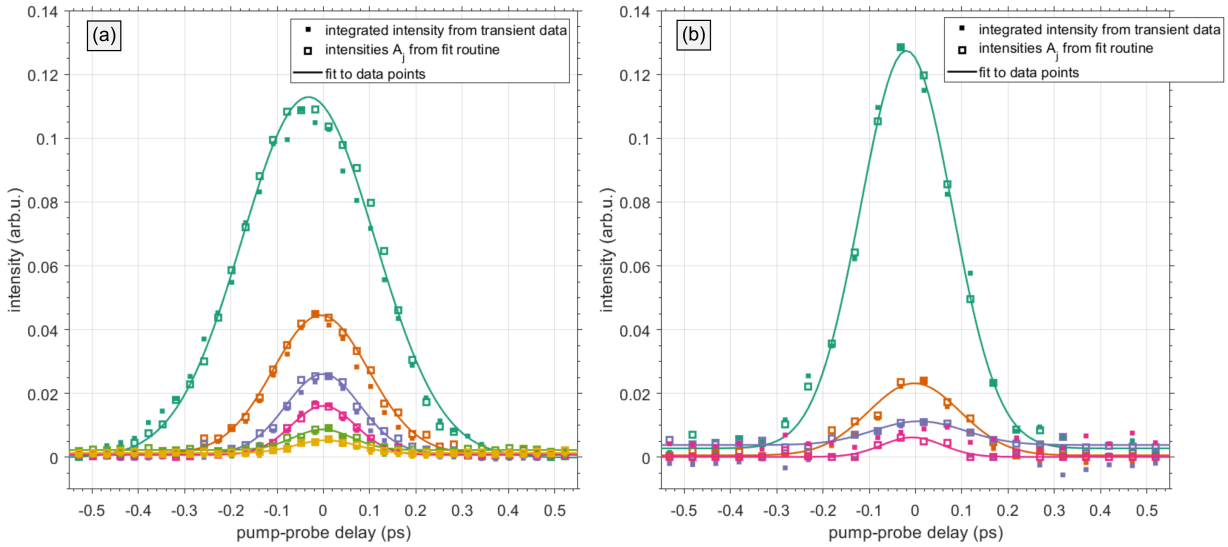

FIG. 2: Lineouts of the transient signal at constant energy intervals associated with SBs for W 4f (a) and Pt 4f (b) generated at exactly same conditions. The solid marker represent the intensity from integration within fixed energy regions (cf. marked areas of the different sidebands as shown in Fig. 1). The open marker display the resulting SB intensities A_j of the fit routine described in detail in the text. The selected color code is identical to that in Fig. 1 and corresponds to the different observed SB orders.

is performed for the W and Pt spectra.

Red lines in Fig. 1 (c) and (d) show the results of the total fit. The individual components for all observed sidebands and the remaining emission line for W 4f and Pt 4f are color-coded, respectively. Moreover, Fig. 2 (a) and (b) show lineouts of the transient signal, extracted from the SB regions marked in Fig. 1 (a) and (b), in comparison to the intensities A_j. The integrated transient data are adjusted in intensity to match the corresponding A_j. Solid lines in Fig. 2 (a) and (b) are the results of fitting the temporal evolution of the A_j parameters with Gaussian functions. The results in Fig. 2 show that the parametrization of the spectra using the RF according to eq. 1 provides an excellent description of the SB spectra for all SB orders and all pump-probe delays.

In order to elucidate the physical origins of the observed trends, we use a theoretical model of short-pulse two-color photoemission based on the Strong Field Approximation [25]. Note that the penetration depth of both pulses is much larger than the electron inelastic mean

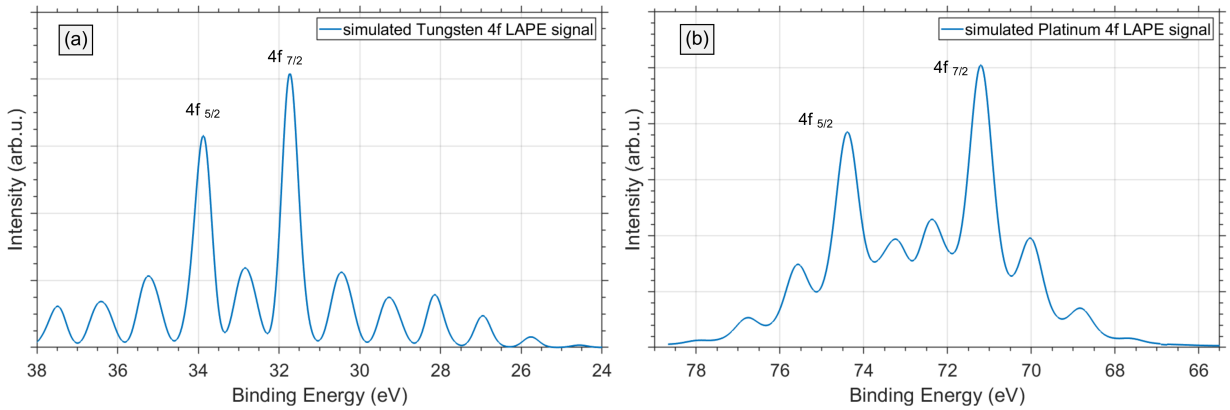

FIG. 3: Simulated photoemission spectrum for W 4f photolines (a) and Pt 4f (b). The spectra are shown for the IR peak intensity of $3 \times 10^{11}\,\mathrm{W/cm^2}$ in case of W and $0.7 \times 10^{11}\,\mathrm{W/cm^2}$ in case of Pt. Details about the simulation can be found in the text and in the Appendix. The energy scale was transfered into binding energy to match the experimental data display.

free path near the metal surface. For both targets the latter is 5 - 7 Å [26]. Therefore only the first few atomic layers contribute to the measured spectra. The emission of an electron from an atom at the surface is considered as a one-step process within the single-active electron approximation.

The electron transits from the initial tightly bound 4f state to the final state in continuum distorted by the IR field. The initial state is described as purely atomic 4f state while the final continuum state is represented by a Volkov wave function [27] which describes the electron moving in the IR field. Details of this approach and the calculations are presented in the Appendix.

Within the theoretical model, the sidebands are the result of interference of electron waves emitted at the same phase of the IR field, but in different periods. The number of the sidebands can be roughly estimated as $2A_L\sqrt{2E_e}/\omega_L$, where A_L is the vector potential of the IR field and ω_L is its frequency. E_e is the kinetic energy of the photoelectron [28]. Within this model, the number of sidebands is proportional to the value of the laser vector potential, which is considered constant in space and only dependent on time. Since the vector potential is the same and the electron kinetic energy is similar for both targets, one would expect that the number of sidebands is also similar.

Considering the vector potential as a variable parameter, we calculated the photoelectron spectra from W and Pt with other parameters similar to the experiment (see Appendix). The calculations show that the IR field applied to W would have to be 3-4 times larger than for Pt in order to obtain spectra comparable to those observed in the experiment (see Fig. 3). Such as variation of the IR intensity is clearly not commensurate with the experiment, where it was kept constant throughout both measurements.

To resolve this discrepancy, we resort to the theory of photoemission from metal surfaces, which was widely discussed toward the end of the last century. It was realized that, in order to describe the experimental photoemission yield, it is necessary to take into account the spatial non-uniformity of the electromagnetic field near the surface [29]. The z component of the vector potential is discontinuous at the surface and the effects of refraction and reflection must be taken into account. The impact of these effects may be roughly estimated by assuming that the sample acts as an isotropic medium of dielectric constant $\epsilon_m(\omega_L)$, having a sharp surface in the plane $z = 0$. In this case, the electric field can be computed using Fresnel equations.

As shown in [30–32], the z-component of the vector potential just below the surface from where the electrons are emitted, may be presented as

$$A_{Lz} = A_0 \frac{2\cos\theta_i \sin\theta_i}{\epsilon_m \cos\theta_i + (\epsilon_m - \sin^2\theta_i)^{1/2}} \tag{2}$$

where A_0 is the amplitude of the IR vector potential of the incident wave, θ_i is the incidence angle of the IR light and ϵ_m is the complex dielectric constant of the solid:

$$\epsilon_m = \epsilon_{1m} + i\epsilon_{2m}. \tag{3}$$

The dielectric constant strongly depends on the IR photon energy. Its tabulated values can be found, for example, in [33]. For the IR photon energy of our experiment the dielectric constants are

$$\epsilon_{1m} = -4.25; \qquad \epsilon_{2m} = 21.8 \qquad \text{for W}$$
$$\epsilon_{1m} = -22.4; \qquad \epsilon_{2m} = 42.0 \qquad \text{for Pt.}$$

Substituting these values into Eq. (2) and taking into account the incidence angle $\theta_i = 55°$ we obtain a ratio of $|A_{Lz}|^2_W / |A_{Lz}|^2_{Pt} = 3.77$ for the normal components of the IR vector potential in the different materials. Therefore, the intensity of the IR field just under the surface is

almost four times larger in W than in Pt. This finding agrees well with the IR intensity ratio identified above by the parametrization model to explain the different sideband numbers.

The presented results show that the influence of an IR driving field for pump-probe experiments induces complex interaction of several influencing factors. Yet, it is also shown that a careful evaluation of these processes is possible and has to be done in order to compare results from different targets. Additionally, one has to take into account that these screening processes also have a temporal component. The LAPE process is dependent on the actual electric field in the surface region, which differs from the intrinsic field of the laser pulse in terms of both its amplitude and its temporal evolution. This offers new insights not only into the spatial, but also the temporal evolution of electronic screening processes at surfaces.

We would like to note that attosecond time-resolved photoemission using the streaking approach has recently been used to gain insight into the propagation and damping of electronic and optical wave packets at solid surfaces like W(110), Mg(0001), or even more complex systems like the Mg/W(110) interface or the van der Waals crystal WSe_2 [34–37]. In all cases, time delays between photoelectrons from different emission channels were recorded and several theoretical studies were published to explain those observations. However, the detailed dielectric response of the sample to the IR laser field was not taken into account in these studies.

The demonstrated sensitivity of the presented femtosecond tr-LAPE measurements to the dielectric properties of the sample in a sub-nm thick surface layer could be exploited to monitor electronic and lattice dynamics in this surface region and provide a deeper understanding of the theory of surface electromagnetic fields including local fields at a chemisorbed atom or molecule. Moreover, using higher X-ray photon energies—larger electron escape depths—one may also be able to probe properties and dynamics at buried interfaces as long as the IR field still reaches these sample regions.

The findings presented here demonstrate that the presence of the laser-assisted photoelectric effect in high-resolution pump-probe core level spectroscopy requires special attention. Yet, the results also provide new opportunities for even more challenging experimental and theoretical investigations utilizing ultrafast and intense laser fields at next-generation high repetition-rate X-ray light sources.

IV. SUMMARY

In summary, we present a systematic investigation of the laser-assisted photoelectric effect in two similar solid materials - W (110) and Pt (111) single crystals. The unexpected difference in the numbers of sidebands generated under the same optical laser and X-ray source conditions can be semi-quantitatively explained by the sensitivity to screening effects and the dynamic dielectric response of solid state materials. Using the strong-field approximation, we show that the intrinsic, near-surface IR laser field enhancement by a factor of four is the root cause for the larger number of sidebands in tungsten compared to platinum.

ACKNOWLEDGMENTS

We acknowledge DESY (Hamburg, Germany), a member of the Helmholtz Association HGF, for the provision of experimental facilities. Beamtime was allocated with the Application ID 11010397. Moreover, we would like to thank the staff at FLASH at DESY for their excellent support during the experiment. We thank H. Meyer and S. Gieschen from University of Hamburg for support with the instrumentation. These experiments were supported within the research program 'structure of matter' of the Helmholtz Gemeinschaft (HGF). F.R. acknowledges financial support from DESY. This work was supported by the BMBF (Grant No. 05K22OF2 within ErUM-Pro). N.M.K. acknowledges the hospitality and financial support from Donistia International Physics Center (DIPC) as well as financial support from European XFEL. He is also grateful to E.E. Krasovskii and V.M. Silkin for many illuminating discussions. M.B. and O.G. were supported by the Atomic, Molecular, and Optical Sciences Program of the U.S. Department of Energy, Office of Science, Office of Basic Energy Sciences, Chemical Sciences, Geosciences and Biosciences Division, through Contract No. DE-AC0205CH11231. N.W. acknowledge funding by the DFG within the framework of the Collaborative Research Centre SFB 925 - 170620586 (project B2).

APPENDIX

A. Strong field approximation

We consider photoionization of an atom at a metallic surface in the field of two pulses: a comparatively weak XUV pulse and a rather strong IR pulse. The pulses co-propagate along the same direction at angle θ_i (measured from a surface normal) and are linearly polarized in a plane of incidence ("p-polarized"). For the description of ionization of the atoms by a combined action of the XUV and the IR fields, we use a well known approach based on the Strong Field Approximation (SFA) [25]. The emission of an electron is considered as a one-step process of transition from the initial bound state to the final continuum state distorted by the IR field. The interaction of the electron with the XUV pulse is described within the first-order time-dependent perturbation approach with usage of the Rotating Wave Approximation (RWA). Within the single-active-electron approximation the ionization amplitude can be presented as [28] (atomic units (a.u.) are used throughout unless otherwise indicated)

$$\mathcal{A}(\vec{k}) \sim -i \int_{-\infty}^{\infty} dt\, \tilde{\mathcal{E}}_X(t) < \psi_{\vec{k}}(t)|\hat{d}|\psi_0 > e^{i(|E_b|-\omega_X)t}\,, \tag{4}$$

where $\tilde{\mathcal{E}}_X(t)$ is the envelope of the XUV pulse, ω_X is its mean frequency, E_b is the binding energy of the electron, $\hat{d}$ is the dipole operator, which describes the interaction of the electron with the XUV field. The function ψ_0 is the initial single-electron wave function. Since in the experiment ionization of an inner atomic shell is studied, we assume that ψ_0 is a localized function of the atomic electron. Thus we ignore a solid-state environment.

The wave function $\psi_{\vec{k}}(t)$ in equation (4) describes the "dressed" photoelectron in the IR field, which is characterized by the final (asymptotic) momentum $\vec{k}$. It is represented by the non-relativistic Volkov wave function [**?**]:

$$\psi_{\vec{k}} = \exp\left\{ i[\vec{k} - \vec{A}_L(t)]\vec{r} - i\Phi_V(\vec{k},t) \right\}\,. \tag{5}$$

Here $\Phi_V(\vec{k},t)$ is the Volkov phase

$$\Phi_V(\vec{k},t) = -\frac{1}{2}\int_t^{\infty} dt' \left[\vec{k} - \vec{A}_L(t')\right]^2 \tag{6}$$

with $\vec{A}_L(t)$ being the vector potential of the IR field, which is defined as $\vec{A}_L(t) = \int_t^{\infty} dt' \vec{\mathcal{E}}_L(t')$, where $\vec{\mathcal{E}}_L(t)$ is the IR electric field vector. As a first approximation we assume that the IR vector potential is spacial constant.

B. Evaluation of the dipole matrix element

In the considered case, the initial electron state is $4f$-state with orbital angular moment $l_0 = 3$. The final continuum state $\psi_{\vec{k}_0}$, where $\vec{k}_0 = \vec{k} - \vec{A}_L(t)$ may be expanded in partial waves. The dipole transition is possible to the "g" and "d" partial waves. Since at high photoelectron energy the transition to the "l_0+1" state dominates, we ignore the transitions to the d-continuum. Then the matrix element in equation (4) for a particular projection of the initial orbital angular momentum m_0 may be presented as

$$< \psi_{\vec{k}_0}(t)|\hat{d}|\psi_{4f,m_0} >\sim e^{i\Phi_V(\vec{k},t)} Y_{4,m_0}(\theta_0,\phi_0)\mathcal{R}^1_{k_0,l_0} C(l,l_0,m_0)\,, \tag{7}$$

where $Y_{l,m_0}(\theta_0,\phi_0)$ is the spherical harmonic, $\mathcal{R}^1_{k_0,l_0}$ and $C(l,l_0,m_0)$ are the radial and angular parts of the matrix element. $C(4,3,m_0) =< Y_{4,m_0}|Y_{1,0}|Y_{3,m_0} >$. The angles (θ_0,ϕ_0) give the direction of electron emission from the atom before propagation in the optical laser field. These angles are connected with the detection angles (θ,ϕ) after propagation in the IR field by the relations:

$$\theta_0(t) = \arcsin(k\sin\theta/k_0(t))\,, \tag{8}$$

$$k_0^2(t) = (\vec{k} - \vec{A}_L(t))^2\,. \tag{9}$$

Substituting the matrix element into the amplitude (4) one gets

$$\mathcal{A}_{m_0}(\vec{k}) \sim -iC_{l,l_0,m_0}\int_{-\infty}^{\infty} dt\; \tilde{\mathcal{E}}_X(t) e^{i\Phi_V(\vec{k},t)}\mathcal{R}^1_{k_0,l_0} Y_{4,m_0}(\hat{k}_0) e^{i(|E_b|-\omega_X)t}\,, \tag{10}$$

which gives for the cross section

$$\frac{d\sigma}{d\Omega}(\vec{k}) = \sum_{m_0} |\mathcal{A}_{m_0}(\vec{k})|^2\,. \tag{11}$$

C. Details of calculations

The envelope of the XUV pulse (electric field) is Gaussian:

$$\tilde{\mathcal{E}}_X = \mathcal{E}_0 e^{-(t-T_{init})^2/T^2_{XUV}} \tag{12}$$

where $T_{XUV} = 3018$ a.u. (duration of the XUV pulse FWHM ~ 80 fs) and $T_{init} = 970$ a.u. (the middle of the IR pulse)

The envelope of the IR pulse (electric field):

$$\tilde{\mathcal{E}}_L = \mathcal{E}_{L0}/(1+e^{(-t/T_0)}) \qquad \text{if } t \leq T_{IR}/2 \tag{13}$$

$$= \mathcal{E}_{L0}/(1+e^{((t-T_{IR})/T_0)}) \qquad \text{if } t \geq T_{IR}/2 \tag{14}$$

where $\mathcal{E}_{L0}$ is a peak value of the IR electric field, $T_0 = 300$ a.u. , $T_{IR} = 1940$ a.u. (duration of the IR pulse FWHM $\sim$ 50 fs). The IR frequency is 0.0441 a.u. (1030 nm). Note, that by calculation reasons, the duration of both pulses is about two times smaller than in the experiment.

At the photon energy 515 eV, the kinetic energy of an electron emitted from 4f subshell of W is taken as 17.5 a.u. (476 eV). No fine-structure splitting is included. For Pt the kinetic energy is 16.17 a.u. (440 eV).

The calculations have been done for an emission angle (with respect to the photon electric field) 35° which corresponds to the normal emission, perpendicular to the surface. Since at high electron energy the radial parts of the dipole matrix elements are slowly varying function of energy, in numerical calculations we consider them as a constant and put them to unity.

The calculated spectra were additionally convoluted with the Gaussian, imitating the energy resolution of the detector and the spectral width of the laser pulse which were assumed to be about 0.4 eV. Additionally, the spectra are convoluted with Lorentian with $\Gamma = 0.06$ eV for W and 0.4 eV for Pt. To imitate the spin-orbit splitting we added to the calculated spectrum its copy shifted in energy by 2.1 eV for W and 3.2 eV for Pt and diminished by factor of 0.75. The resulting spectra are shown in Fig 3.

---

[1] F. Roth, M. Borgwardt, L. Wenthaus, J. Mahl, S. Palutke, G. Brenner, G. Mercurio, S. Molodtsov, W. Wurth, O. Gessner, and W. Eberhardt, "Direct observation of charge separation in an organic light harvesting system by femtosecond time-resolved XPS," Nature Communications **12**, 1196 (2021).

[2] M. Borgwardt, J. Mahl, F. Roth, L. Wenthaus, F. Brauße, M. Blum, K. Schwarzburg, G. Liu, F. M. Toma, and O. Gessner, "Photoinduced Charge Carrier Dynamics and Electron Injection Efficiencies in Au Nanoparticle-Sensitized TiO2 Determined with Picosecond Time-Resolved X-ray Photoelectron Spectroscopy," J. Phys. Chem. Lett. , 5476–5481 (2020).

[3] J. M. Schins, P. Breger, P. Agostini, R. C. Constantinescu, H. G. Muller, G. Grillon, A. Antonetti, and A. Mysyrowicz, "Observation of laser-assisted auger decay in argon," Phys. Rev. Lett. **73**, 2180–2183 (1994).

[4] T. E. Glover, R. W. Schoenlein, A. H. Chin, and C. V. Shank, "Observation of laser assisted photoelectric effect and femtosecond high order harmonic radiation," Phys. Rev. Lett. **76**, 2468–2471 (1996).

[5] L. Cattaneo, J. Vos, M. Lucchini, L. Gallmann, C. Cirelli, and U. Keller, "Comparison of attosecond streaking and RABBIT," Opt. Express **24**, 29060–29076 (2016).

[6] M. Lucchini, L. Castiglioni, L. Kasmi, P. Klieuiev, A. Ludwig, M. Greif, J. Osterwald, M. Hengsberger, L. Gallmann, and U. Keller, "Light-matter interaction at surfaces in the spatiotemporal limit of macroscopic models," Phys. Rev. Lett. **115**, 137401 (2015).

[7] F. Mahmood, C.-K. Chan, Z. Alpichshev, D. Gardner, Y. Lee, P. A. Lee, and N. Gedik, "Selective scattering between Floquet–Bloch and Volkov states in a topological insulator," Nature Physics **12**, 1306–310 (2016).

[8] L. Miaja-Avila, C. Lei, M. Aeschlimann, J. L. Gland, M. M. Murnane, H. C. Kapteyn, and G. Saathoff, "Laser-Assisted Photoelectric Effect from Surfaces," Phys. Rev. Lett. **97**, 113604 (2006).

[9] A Pietzsch, A Föhlisch, M Beye, M Deppe, F Hennies, M Nagasono, E Suljoti, W Wurth, C Gahl, K Döbrich, and A Melnikov, "Towards time resolved core level photoelectron spectroscopy with femtosecond x-ray free-electron lasers," New J. Phys. **10**, 033004 (2008).

[10] M. Meyer, D. Cubaynes, P. O'Keeffe, H. Luna, P. Yeates, E. T. Kennedy, J. T. Costello, P. Orr, R. Taïeb, A. Maquet, S. Düsterer, P. Radcliffe, H. Redlin, A. Azima, E. Plönjes, and J. Feldhaus, "Two-color photoionization in xuv free-electron and visible laser fields," Phys. Rev. A **74**, 011401 (2006).

[11] M. Seidel, F. Pressacco, O. Akcaalan, T Binhammer, J. Darvill, N. Ekanayake, M. Frede, U. Grosse-Wortmann, M Heber, C.M. Heyl, D. Kutnyakhov, C. Li, C. Mohr, J. Müller, O. Puncken, H. Redlin, N. Schirmel, S. Schulz, A. Swiderski, H. Tavakol, H. Tünnermann, C Vidoli, L. Wenthaus, N. Wind, L. Winkelmann, B. Manschwetus, and I. Hartl, "Ultrafast mhz-rate burst-mode pump–probe laser for the flash fel facility based on nonlinear compression of ps-level pulses from an yb-amplifier chain," Laser Photonics Reviews **16**, 2100268 (2022).

[12] A Azima, S Düsterer, P. Radcliffe, H Redlin, N Stojanovic, W Li, H Schlarb, J Feldhaus,

D Cubaynes, M Meyer, J Dardis, P Hayden, P Hough, V Richardson, E T Kennedy, and J T Costello, "Time-resolved pump-probe experiments beyond the jitter limitations at flash," Appl. Phys. Lett. **24**, 144102 (2009).

[13] P. Finetti, H. Höppner, E. Allaria, C. Callegari, F. Capotondi, P. Cinquegrana, M. Coreno, R. Cucini, M. B. Danailov, A. Demidovich, G. De Ninno, M. Di Fraia, R. Feifel, E. Ferrari, L. Fröhlich, D. Gauthier, T. Golz, C. Grazioli, Y. Kai, G. Kurdi, N. Mahne, M. Manfredda, N. Medvedev, I. P. Nikolov, E. Pedersoli, G. Penco, O. Plekan, M. J. Prandolini, K. C. Prince, L. Raimondi, P. Rebernik, R. Riedel, E. Roussel, P. Sigalotti, R. Squibb, N. Stojanovic, S. Stranges, C. Svetina, T. Tanikawa, U. Teubner, V. Tkachenko, S. Toleikis, M. Zangrando, B. Ziaja, F. Tavella, and L. Giannessi, "Pulse Duration of Seeded Free-Electron Lasers," Phys. Rev. X **7**, 021043 (2017).

[14] T. Arion, S. Neppl, F. Roth, A. Shavorskiy, H. Bluhm, Z. Hussain, O. Gessner, and W. Eberhardt, "Site-specific probing of charge transfer dynamics in organic photovoltaics," Appl. Phys. Lett. **106**, 121602 (2015).

[15] F. Roth, S. Neppl, A. Shavorskiy, T. Arion, J. Mahl, H. O. Seo, H. Bluhm, Z. Hussain, O.r Gessner, and W. Eberhardt, "Efficient charge generation from triplet excitons in metal-organic heterojunctions," Phys. Rev. B **99**, 020303 (2019).

[16] S. Neppl, J. Mahl, F. Roth, G. Mercurio, G. Zeng, F. M. Toma, N. Huse, P. Feulner, and O. Gessner, "Nanoscale Confinement of Photo-Injected Electrons at Hybrid Interfaces," J. Phys. Chem. Lett. **12**, 11951–11959 (2021).

[17] G. Saathoff, L. Miaja-Avila, M. Aeschlimann, M. M. Murnane, and H. C. Kapteyn, "Laser-assisted photoemission from surfaces," Phys. Rev. A **77**, 022903 (2008).

[18] W. Ackermann, G. Asova, V. Ayvazyan, A. Azima, N. Baboi, J. Bähr, V. Balandin, B. Beutner, A. Brandt, A. Bolzmann, R. Brinkmann, O. I. Brovko, M. Castellano, P. Castro, L. Catani, E. Chiadroni, S. Choroba, A. Cianchi, J. T. Costello, D. Cubaynes, J. Dardis, W. Decking, H. Delsim-Hashemi, A. Delserieys, G. Di Pirro, M. Dohlus, S. Düsterer, A. Eckhardt, H.T. Edwards, B. Faatz, J. Feldhaus, K. Flöttmann, J. Frisch, L. Fröhlich, T. Garvey, U. Gensch, Ch. Gerth, M. Görler, N. Golubeva, H.-J. Grabosch, M. Grecki, O. Grimm, K. Hacker, U. Hahn, J. H. Han, K. Honkavaara, T. Hott, M. Hüning, Y. Ivanisenko, E. Jaeschke, W. Jalmuzna, T. Jezynski, R. Kammering, V. Katalev, K. Kavanagh, E. T. Kennedy, S. Khodyachykh, K. Klose, V. Kocharyan, M. Körfer, M. Kollewe, W. Koprek,

S. Korepanov, D. Kostin, M. Krassilnikov, G. Kube, M. Kuhlmann, C. L. S. Lewis, L. Lilje, T. Limberg, D. Lipka, F. Löhl, H. Luna, M. Luong, M. Martins, M. Meyer, P. Michelato, V. Miltchev, W. D. Möller, L. Monaco, W. F. O. Müller, O. Napieralski, O. Napoly, P. Nicolosi, D. Nölle, T. Nuñez, A. Oppelt, C. Pagani, R. Paparella, N. Pchalek, J. Pedregosa-Gutierrez, B. Petersen, B. Petrosyan, G. Petrosyan, L. Petrosyan, J. Pflüger, E. Plönjes, L. Poletto, K. Pozniak, E. Prat, D. Proch, P. Pucyk, P. Radcliffe, H. Redlin, K. Rehlich, M. Richter, M. Roehrs, J. Roensch, R. Romaniuk, M. Ross, J. Rossbach, V. Rybnikov, M. Sachwitz, E. L. Saldin, W. Sandner, H. Schlarb, B. Schmidt, M. Schmitz, P. Schmüser, J. R. Schneider, E. A. Schneidmiller, S. Schnepp, S. Schreiber, M. Seidel, D. Sertore, A. V. Shabunov, C. Simon, S. Simrock, E. Sombrowski, A. A. Sorokin, P. Spanknebel, R. Spesyvtsev, L. Staykov, B. Steffen, F. Stephan, F. Stulle, H. Thom, K. Tiedtke, M. Tischer, T. Toleikis, R. Treusch, D. Trines, I. Tsakov, E. Vogel, T. Weiland, H. Weise, M. Wellhöfer, M. Wendt, I. Will, A. Winter, K. Wittenburg, W. Wurth, P. Yeates, M. V. Yurkov, Zagorodnov I., and K. Zapfe, "Operation of a free-electron laser from the extreme ultraviolet to the water window." Nature Photonics **1**, 336–342 (2007).

[19] M. Martins, M. Wellhöfer, J. T. Hoeft, W. Wurth, J. Feldhaus, and R. Follath, "Monochromator beamline for FLASH," Review of Scientific Instruments **77**, 115108 (2006).

[20] N. Gerasimova, S. Dziarzhytski, and J. Feldhaus, "The monochromator beamline at FLASH: performance, capabilities and upgrade plans," Journal of Modern Optics **58**, 1480–1485 (2011).

[21] M. Keunecke, M. Reutzel, D. Schmitt, A. Osterkorn, T. A. Mishra, C. Möller, W. Bennecke, G. S. M. Jansen, D. Stiel, S. R. Manmana, S. Steil, S. Kehrein, and Mathias S., "Electromagnetic dressing of the electron energy spectrum of au(111) at high momenta," Phys. Rev. B. **102**, 161403 (2020).

[22] L.-P. Oloff, M. Oura, K. Rossnagel, A. Chainani, M. Matsunami, R. Eguchi, T. Kiss, Y. Nakatani, T. Yamaguchi, J. Miyawaki, M. Taguchi, K. Yamagami, T. Togashi, T. Katayama, K. Ogawa, M. Yabashi, and T. Ishikawa, "Time-resolved haxpes at sacla: probe and pump pulse-induced space-charge effects," New Journal of Physics **12** (2014).

[23] J. L. Campbell and T. Papp, "Widths of the atomic k–n7 levels," Atomic Data and Nuclear Data Tables **77**, 1–56 (2001).

[24] S. Doniach and M. Sunjic, "Many-electron singularity in x-ray photoemission and x-ray line spectra from metals," Journal of Physics C: Solid State Physics **3**, 285 (1969).

[25] L.V. Keldysh, "Ionization in the field of a strong electromagnetic wave," Sov. Phys. JETP **20**, 1307 (1965).

[26] C. J. Powell and A. Jablonski, "Evaluation of calculated and measured electron inelastic mean free paths near solid surfaces," J. Phys. Chem. Ref. Data **28**, 19–62 (1999).

[27] D. M. Wolkow, "Über eine Klasse von Lösungen der Diracschen Gleichung," Z. Physik **94**, 250–260 (1935).

[28] A. K. Kazansky, I. P. Sazhina, and N. M. Kabachnik, "Angle-resolved electron spectra in short-pulse two-color xuv+ir photoionization of atoms," Phys. Rev. A **82**, 033420 (2010).

[29] Harry J. Levinson, E. W. Plummer, and P. J. Feibelman, "Effects on photoemission of the spatially varying photon field at a metal surface," Phys. Rev. Lett. **43**, 952–955 (1979).

[30] P. J. Feibelman, "Comment on recent theories of photoemission," Surface Science **46**, 558–566 (1974).

[31] M. A. B. Whitaker, "Use of the fresnel equations in the theory of angle-resolved photoemission," J. Phys. C: Solid State Phys. **11**, L151 (1978).

[32] P. J. Feibelman, "Surface electromagnetic fields," Progress in Surface Science **12**, 287–407 (1982).

[33] S. Adachi, *The Handbook on Optical Constants of Metals* (World Scientific, 2012).

[34] A. L. Cavalieri, N. Müller, Th. Uphues, V. S. Yakovlev, A. Baltuška, B. Horvath, B. Schmidt, L. Blümel, R. Holzwarth, S. Hendel, M. Drescher, U. Kleineberg, P. M. Echenique, R. Kienberger, F. Krausz, and U. Heinzmann, "Attosecond spectroscopy in condensed matter," Nature **449**, 1029–1032 (2007).

[35] S. Neppl, R. Ernstorfer, A. L. Cavalieri, C. Lemell, G. Wachter, E. Magerl, E. M. Bothschafter, M. Jobst, M. Hofstetter, U. Kleineberg, J. V. Barth, D. Menzel, J. Burgdörfer, P. Feulner, F. Krausz, and R. Kienberger, "Direct observation of electron propagation and dielectric screening on the atomic length scale," Nature **517**, 342–346 (2015).

[36] S. Neppl, R. Ernstorfer, E. M. Bothschafter, A. L. Cavalieri, D. Menzel, J. V. Barth, F. Krausz, R. Kienberger, and P. Feulner, "Attosecond time-resolved photoemission from core and valence states of magnesium," Phys. Rev. Lett. **109**, 087401 (2012).

[37] F. Siek, S. Neb, P. Bartz, M. Hensen, C. Strüber, S. Fiechter, M. Torrent-Sucarrat, V. M. Silkin, E. E. Krasovskii, N. M. Kabachnik, S. Fritzsche, R. Díez Muiño, P. M. Echenique, A. K. Kazansky, N. Müller, W. Pfeiffer, and U. Heinzmann, "Angular momentum-induced delays

in solid-state photoemission enhanced by intra-atomic interactions," Science **357**, 1274–1277 (2017).